



LAWRENCE
LIVERMORE
NATIONAL
LABORATORY

Progress with the COGENT Edge Kinetic Code: Implementing the Fokker-Plank Collision Operator

M. Dorf, R. Cohen, M. Dorr, J. Hittinger, T. Rognien

September 17, 2013

Contributions to Plasma Physics

Disclaimer

This document was prepared as an account of work sponsored by an agency of the United States government. Neither the United States government nor Lawrence Livermore National Security, LLC, nor any of their employees makes any warranty, expressed or implied, or assumes any legal liability or responsibility for the accuracy, completeness, or usefulness of any information, apparatus, product, or process disclosed, or represents that its use would not infringe privately owned rights. Reference herein to any specific commercial product, process, or service by trade name, trademark, manufacturer, or otherwise does not necessarily constitute or imply its endorsement, recommendation, or favoring by the United States government or Lawrence Livermore National Security, LLC. The views and opinions of authors expressed herein do not necessarily state or reflect those of the United States government or Lawrence Livermore National Security, LLC, and shall not be used for advertising or product endorsement purposes.

Progress with the COGENT Edge Kinetic Code: Implementing the Fokker-Plank Collision Operator

M. A. Dorf*, R. H. Cohen, M. Dorr, J. Hittinger, and T. D. Rognlien

Lawrence Livermore National Laboratory, Livermore, CA 94550 USA

Received *** September 2013, revised *** 2013, accepted *** 2013

Published online *** 2013

Key words Edge, plasma, simulation, kinetic, gyrokinetic.

PACS 52.65.Tt, 52.55.Rk, 52.65.-y, 52.25.Dg, 52.55.Fa

COGENT is a continuum gyrokinetic code for edge plasma simulations being developed by the Edge Simulation Laboratory collaboration. The code is distinguished by application of a fourth-order finite-volume (conservative) discretization, and mapped multiblock grid technology to handle the geometric complexity of the tokamak edge. The distribution function F is discretized in $v_{\parallel} - \mu$ (parallel velocity – magnetic moment) velocity coordinates, and the code presently solves an axisymmetric full- f gyro-kinetic equation coupled to the long-wavelength limit of the gyro-Poisson equation. COGENT capabilities are extended by implementing the fully nonlinear Fokker-Plank operator to model Coulomb collisions in magnetized edge plasmas. The corresponding Rosenbluth potentials are computed by making use of a finite-difference scheme and multipole-expansion boundary conditions. Details of the numerical algorithms and results of the initial verification studies are discussed.

Copyright line will be provided by the publisher

1 Introduction

The edge of a tokamak is distinguished by a complex magnetic geometry and short radial length scales (comparable to particle drift-orbit excursion) for plasma density and temperature variations. Also, the gradient length scales along the magnetic field can be comparable to collisional mean free path. As a result, substantial deviations from a local Maxwellian distribution can occur, and a full- f kinetic code including the nonlinear Fokker-Plank (FP) collision operator is required for adequate modeling of edge plasmas. To avoid the critical problem of statistical noise in full- f PIC simulations, the Edge Simulation Laboratory (ESL) collaboration has developed a continuum gyro-kinetic code COGENT [1-4], which discretizes a kinetic equation on a phase-space grid and employs advanced numerical methods from fluids community [4-5]. COGENT utilizes a fourth-order finite-volume (conservative) discretization combined with arbitrary mapped multiblock grid technology (flux surface aligned on blocks) to handle the complexity of tokamak divertor geometry with high accuracy [4-6]. The present version of the code models an axisymmetric 4D ($\mathbf{R}, v_{\parallel}, \mu$) gyrokinetic equation coupled to the long-wavelength limit of the gyro-Poisson equation. Here, \mathbf{R} denotes the gyrocenter coordinate in the poloidal plane, and v_{\parallel} and μ are the gyrocenter velocity parallel to the magnetic field and the magnetic moment, respectively. In our previous studies, we discussed the implementation of various simplified collision models [1] and their performance in neoclassical simulations [2]. In this work, we report on the implementation and initial testing of the fully nonlinear Fokker-Plank collision operator.

Evaluation of the Fokker-Plank operator requires computation of the so-called Rosenbluth potentials determined by two coupled elliptic (Poisson) equations in the velocity space. A widely used approach for evaluation of the Rosenbluth potentials in magnetized plasmas involves decomposition of a distribution function using Legendre polynomials of the v_{\parallel}/v coordinate [7-9]. Here, $v=|\mathbf{v}|$ denotes the particle speed. Recently, Pataki and Greengard proposed an alternative spectral method [10], which employs fast Fourier transforms in the v_{\parallel} -direction allowing for very efficient (fast) computation of the Rosenbluth potentials. While such spectral methods

* Corresponding author: e-mail: dorf1@llnl.gov, Phone: +1 925 422 5181, Fax: +1 925 423 3484

exhibit rapid convergence for smooth velocity distributions characteristic of a tokamak core, the presence of velocity-space holes (due to prompt orbit loss) in a tokamak edge can substantially degrade their convergence properties. To make use of the advanced grid technologies implemented in COGENT [4-6], which will allow for efficient adaptive-mesh-refinement (AMR) treatment of the velocity distributions in a tokamak edge, we develop a finite-difference algorithm to solve for the Rosenbluth potentials. Note that iterative schemes used for solving such finite-difference approximations can benefit from a good initial guess, for which a solution from a previous time-step can be used.

Evaluation of the Rosenbluth potentials requires solving the Poisson equations in the open velocity space, and therefore appropriate boundary conditions should be computed for a finite-domain simulation. While the free-space (radiation) boundary condition can be naturally implemented when spectral decomposition is involved [9-10], a finite-difference approach requires the use of the free-space Green's function method to compute the Rosenbluth potentials at the domain boundaries. A direct calculation of the Green's function integrals, however, involves $O(N^{3/2})$ work, and thus can be computationally more intensive than an iterative solve [11-12]. Here, N is the number of velocity grid points used to represent the distribution function. Therefore, we develop an approximate method for a fast calculation of the boundary conditions. The method is based on the multipole expansion of the Green's function, and can be highly effective provided the velocity domain boundaries are placed sufficiently far outside the particle distribution.

The paper is organized as follows: The theoretical model of the Fokker-Plank collision operator is summarized in Sec. II. Details of the simulation model including the multipole-expansion boundary conditions and their implementation are discussed in Sec. III. Finally, the results of initial verification studies are presented in Sec. IV.

2 Fokker-Plank collision operator

Neglecting finite-Larmor-radius effects and considering, for simplicity, single-species collisions, the Fokker-Plank operator takes on the following form in the (v_{\parallel}, μ) coordinates

$$C[F] = L \left(\frac{\partial \Gamma_{v_{\parallel}}}{\partial v_{\parallel}} + \frac{\partial \Gamma_{\mu}}{\partial \mu} \right). \quad (1)$$

Here, $F(\mathbf{R}, v_{\parallel}, \mu)$ is a gyrocenter distribution function, $L = \lambda_c (4\pi q^2/m)^2$ is the logarithmic factor, λ_c denotes the Coulomb logarithm, and q and m correspond to the species charge and mass, respectively. The collisional fluxes in Eq. (1) are given by

$$\Gamma_{v_{\parallel}} = A_{v_{\parallel}} F + D_{v_{\parallel} v_{\parallel}} \frac{\partial F}{\partial v_{\parallel}} + D_{v_{\parallel} \mu} \frac{\partial F}{\partial \mu}, \quad (2)$$

$$\Gamma_{\mu} = A_{\mu} F + D_{\mu v_{\parallel}} \frac{\partial F}{\partial v_{\parallel}} + D_{\mu \mu} \frac{\partial F}{\partial \mu}, \quad (3)$$

and the corresponding drag-diffusion coefficients are specified as

$$A_{v_{\parallel}} = \frac{\partial H}{\partial v_{\parallel}}, \quad A_{\mu} = 2 \frac{m}{B} \mu \frac{\partial H}{\partial \mu}, \quad D_{v_{\parallel} v_{\parallel}} = -\frac{\partial^2 G}{\partial v_{\parallel}^2}, \quad D_{\mu \mu} = -2 \frac{m^2}{B^2} \mu \left(2 \mu \frac{\partial^2 G}{\partial \mu^2} + \frac{\partial G}{\partial \mu} \right), \quad D_{v_{\parallel} \mu} = D_{\mu v_{\parallel}} = -2 \frac{m}{B} \mu \frac{\partial^2 G}{\partial \mu \partial v_{\parallel}}. \quad (4)$$

Here, B is the magnetic field strength, and the Rosenbluth potentials H and G are determined from

$$\frac{\partial^2 H}{\partial v_{\parallel}^2} + \frac{m}{B} \frac{\partial}{\partial \mu} \left(2 \mu \frac{\partial H}{\partial \mu} \right) = F, \quad (5)$$

$$\frac{\partial^2 G}{\partial v_{\parallel}^2} + \frac{m}{B} \frac{\partial}{\partial \mu} \left(2 \mu \frac{\partial G}{\partial \mu} \right) = H. \quad (6)$$

Note that Eqs. (5)-(6) represent the Poisson equations in the 3D velocity space, i.e., $\Delta_v H = F$ and $\Delta_v G = H$, written in the (v_{\parallel}, μ) coordinates for the case where the gyro-angle dependence is ignored.

3 Simulation model

COGENT adopts the standard numerical algorithms developed as part of the Hydre library [31] for solving Eqs. (5)-(6). These algorithms require specification of the Rosenbluth potentials at the boundaries of the simulation domain. Making use of the free-space Green's functions method, it is straightforward to show that the Rosenbluth potentials at the domain boundaries are given by

$$H(\mathbf{v}_{bnd}) = -\frac{1}{4\pi} \int_{\Omega_\infty} \frac{F(\mathbf{v}')}{|\mathbf{v}_{bnd} - \mathbf{v}'|} d^3\mathbf{v}', \quad (7)$$

$$G(\mathbf{v}_{bnd}) = -\frac{1}{8\pi} \int_{\Omega_\infty} |\mathbf{v}_{bnd} - \mathbf{v}'| F(\mathbf{v}') d^3\mathbf{v}', \quad (8)$$

where, \mathbf{v}_{bnd} is the velocity coordinate at the domain boundary, and Ω_∞ denotes the infinite 3D velocity space. As mentioned earlier, the computational work required for direct calculations of the integrals in Eqs. (7) and (8) can be more intensive than that required to solve Eqs. (5)-(6). Therefore, we develop an asymptotic method, based on the multipole-expansion analysis, which can significantly reduce the computational work required to evaluate the boundary conditions in Eqs. (7)-(8).

3.1 Multipole-expansion boundary conditions for the first Rosenbluth potential H

The implementation of the multipole-expansion boundary conditions for the first Rosenbluth potential is straightforward and is based on the expansion of the Green's function in Eq. (7) in spherical harmonics [14],

$$\frac{1}{|\mathbf{v} - \mathbf{v}'|} = 4\pi \sum_{l=0}^{\infty} \sum_{m=-l}^l \frac{1}{2l+1} \frac{v_{<}^l}{v_{>}^{l+1}} Y_{lm}^*(\theta', \varphi') Y_{lm}(\theta, \varphi). \quad (9)$$

Here, Y_{lm} is the spherical harmonic function, $\theta = \arccos(v_{\parallel}/v)$ is the pitch angle, φ is the gyro-angle, $v_{>} = \max\{|\mathbf{v}|, |\mathbf{v}'|\}$, and $v_{<} = \min\{|\mathbf{v}|, |\mathbf{v}'|\}$. Making use of Eqs. (9) and (7), it follows that

$$H(\mathbf{v}_{bnd}) = -\frac{1}{4\pi} \sum_{l=0}^{\infty} \frac{h_l}{|\mathbf{v}_B|^{l+1}} P_l(\cos \theta), \quad (10)$$

where P_l are the Legendre polynomials, and the multipole moments h_l are given by

$$h_l = \frac{2\pi B}{m} \int_{\Omega_c} F(v_{\parallel}, \mu) v^l P_l(\cos \theta) dv_{\parallel} d\mu. \quad (11)$$

Here, Ω_c is the computational $v_{\parallel} - \mu$ domain, $v = |\mathbf{v}|$ denotes the particle speed, and it is assumed that the distribution function F is zero for $|\mathbf{v}| > V_{min}$, where $V_{min} \equiv \min\{|\mathbf{v}_{bnd}|\}$ is the minimal absolute value of the velocity coordinate on the computational domain boundary, $\partial\Omega_c$. Note that the COGENT velocity grid is represented by a uniform rectangular grid, and $|\mathbf{v}_{bnd}|$ varies along the domain boundary.

Equations (10)-(11) constitute the multipole-expansion boundary conditions for the first Rosenbluth potential, H . Note that the multipole moments [Eq. (11)] correspond to the decomposition of a distribution function in the Legendre polynomial basis, and therefore may have degraded decaying properties in a tokamak edge (as discussed in Sec. I). However, fast convergence of the multipole-expansion boundary conditions [in Eq. (10)] is mediated by the presence of $1/v^{l+1}$ coefficients, which exhibit rapid decay for the case where the domain boundary is located sufficiently far from the core of the distribution function.

3.2 Multipole-expansion boundary conditions for the second Rosenbluth potential G

The second Rosenbluth potential is also determined from the Poisson equation with the right-hand-side given by the first Rosenbluth potential, i.e., $\Delta_v G = H$ (see Sec. II). Therefore, by analogy with Eq. (7), it readily follows that

$$G(\mathbf{v}_{bnd}) = -\frac{1}{4\pi} \int_{\Omega_\infty} \frac{H(\mathbf{v}')}{|\mathbf{v}_{bnd} - \mathbf{v}'|} d^3\mathbf{v}'. \quad (12)$$

However, the analysis described in Sec. 3.1 for the case of the first Rosenbluth potential cannot be directly applied

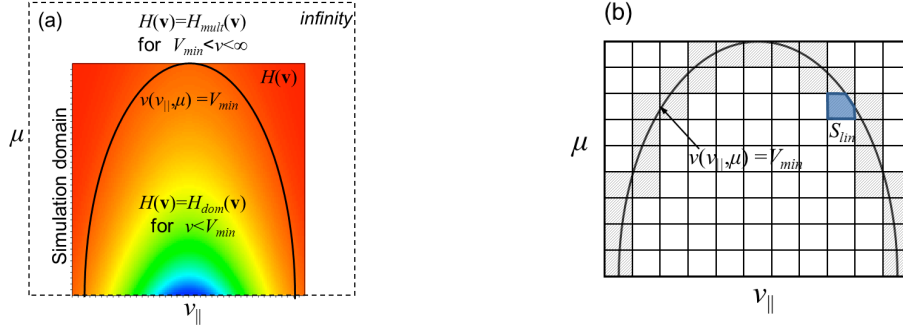


Fig. 1 Implementation of the multipole-expansion boundary conditions. (a) Schematic of the first Rosenbluth potential, $H(\mathbf{v})$, decomposition used for the evaluation of the free-space Green's function integral [in Eqs. (12) and (13)]. (b) Schematic of the cut-cell issue.

to Eq. (12). The difference appears due to the fact that the first Rosenbluth potential $H(\mathbf{v})$ in Eq. (12) is a slowly decaying function, $H \sim 1/v$, whereas the distribution function $F(\mathbf{v})$ in Eq. (7) decays rapidly for typical plasma physics problems, e.g., $F \sim \exp[-(v/v_{th})^2]$. Accordingly, while the distribution function $F(\mathbf{v})$ satisfies the condition of zero (or, negligibly small) $F(\mathbf{v})$ for $|\mathbf{v}| > V_{min}$ within the computational domain, the same is not true for $H(\mathbf{v})$. Moreover, it is straightforward to show that neglecting a slowly decaying tail of $H(\mathbf{v})$ outside some arbitrary large (but finite) domain (with rectangular boundaries in v_{\parallel} and μ) will lead to an erroneous computation of $G(\mathbf{v})$. Therefore, in order to evaluate the multipole-expansion boundary conditions for the second Rosenbluth potential on a compact computational domain, we decompose the integral in Eq. (12) as [see Fig. 1(a)]

$$\int_{\Omega_{\infty}} \frac{H(\mathbf{v}')}{|\mathbf{v}_{bnd} - \mathbf{v}'|} d^3\mathbf{v}' = \int_0^{V_{min}} v^2 dv \int_0^{\pi} d\theta \int_0^{2\pi} d\varphi \frac{H_{dom}(\mathbf{v}')}{|\mathbf{v}_{bnd} - \mathbf{v}'|} + \int_{V_{min}}^{\infty} v^2 dv \int_0^{\pi} d\theta \int_0^{2\pi} d\varphi \frac{H_{mult}(\mathbf{v}')}{|\mathbf{v}_{bnd} - \mathbf{v}'|}. \quad (13)$$

where $H_{dom}(\mathbf{v})$ is the numerical solution for the first Rosenbluth potential [in Eqs. (5), (10), and (11)] on the computational domain, and $H_{mult}(\mathbf{v})$ is the multipole expansion of $H(\mathbf{v})$, i.e.,

$$H_{mult}(\mathbf{v}) = -\frac{1}{4\pi} \sum_{l=0}^{\infty} \frac{h_l}{|\mathbf{v}|^{l+1}} P_l(\cos\theta). \quad (14)$$

Following the analysis in Sec. 3.1 we can now represent the first term on the right-hand-side of Eq. (13) as

$$\int_0^{V_{min}} v^2 dv \int_0^{\pi} d\theta \int_0^{2\pi} d\varphi \frac{H_{dom}(\mathbf{v}')}{|\mathbf{v}_{bnd} - \mathbf{v}'|} = \sum_{l=0}^{\infty} \frac{g_l}{|\mathbf{v}_{bnd}|^{l+1}} P_l(\cos\theta), \quad (15)$$

where the multipole moments g_l are given by

$$g_l = \frac{2\pi B}{m} \int_{\Omega_c} \hat{H}_{dom}(\mathbf{v}_{\parallel}, \mu) v^l P_l(\cos\theta) dv_{\parallel} d\mu, \quad (16)$$

and $\hat{H}_{dom}(\mathbf{v})$ is defined by $\hat{H}_{dom}(\mathbf{v}) = H_{dom}(\mathbf{v})$ for $v \leq V_{min}$ and $\hat{H}_{dom}(\mathbf{v}) = 0$ for $v > V_{min}$. Making use of Eqs. (9) and (14), it is straightforward to show that the second term on the right-hand-side of Eq. (13) can be represented as

$$\int_{V_{min}}^{\infty} v^2 dv \int_0^{\pi} d\theta \int_0^{2\pi} d\varphi \frac{H_{mult}(\mathbf{v}')}{|\mathbf{v}_{bnd} - \mathbf{v}'|} = -\sum_{l=0}^{\infty} \frac{h_l P_l(\cos\theta)}{2l+1} \left(\frac{1}{2|\mathbf{v}_{bnd}|^{l-1}} - \frac{1}{2|\mathbf{v}_{bnd}|^{l+1}} + \frac{1}{2l-1} \frac{1}{|\mathbf{v}_{bnd}|^{l-1}} \right). \quad (17)$$

Note that in deriving Eq. (17) we ignored the diverging contribution from the upper-limit (i.e., $v \rightarrow \infty$) of v -integration for $l=0$ because it only contributes an arbitrary constant to the free-space solution of Eq. (5). This constant vanishes when the drag-diffusion coefficients in Eq. (4) are evaluated, and therefore can be ignored. Collecting the results in Eqs. (15)-(17), we readily obtain

$$G(\mathbf{v}_{bnd}) = -\frac{1}{4\pi} \sum_{l=0}^{\infty} \left[\frac{g_l}{|\mathbf{v}_{bnd}|^{l+1}} - \frac{h_l}{4l+2} \left(\frac{2l+1}{(2l-1)|\mathbf{v}_{bnd}|^{l-1}} - \frac{V_{min}^2}{|\mathbf{v}_{bnd}|^{l+1}} \right) \right] P_l(\cos\theta). \quad (18)$$

3.3 Implementation

Presently, a second-order discretization scheme is employed to evaluate the Rosenbluth potentials in Eqs. (5)-(6) subject to the boundary conditions in Eqs. (10)-(11), (16), and (18). Note that for this order of discretization the cut-cell issues [Fig. 1(b)] associated with the evaluation of the integral in Eq. (16) do not introduce a significant challenge. The contribution to the integral in Eq. (16) from the cut cells is the order $O(N^{-1/2})$. Therefore, the second-order accurate representation of the cut-cell contributions can be achieved by calculating the integral in Eq. (16) over a cut cell as $(2\pi B/m)K_{cc}S_{lin}$. Here, K_{cc} is the cell-centered value of the integrand in Eq. (16) with $H_{dom}(\mathbf{v})$ being used instead of $\hat{H}_{dom}(\mathbf{v})$, and S_{lin} is the part of the cell area lying under the curve $v=V_{min}$, where the curve shape is approximated (within the cell) by a straight line [Fig. 1(b)].

A fourth-order finite volume method is then used to evaluate the Fokker-Plank operator in Eqs. (1)-(4). Note that the resulting accuracy of a simulation corresponds to the accuracy of the lowest-order algorithm involved in the numerical implementation, and is, therefore, presently only of second order. Improving the order of a discretization scheme for the Rosenbluth potentials evaluation (from 2nd order to 4th order) involves more detailed analysis of the cut-cell issues and is currently underway.

4 Results of initial testing

Several initial verification studies of the Fokker-Plank collision model employed in COGENT are reported. Figures 2 and 3 illustrate the results of the Rosenbluth potentials evaluation. For the test-case presented in Fig. 2, we adopt an isotropic normalized distribution function $\bar{F}(\bar{\mathbf{v}})$ [Fig. 2(a)] defined by $\bar{F}(\bar{\mathbf{v}})=1-|\bar{\mathbf{v}}|^2$ for $|\bar{\mathbf{v}}|\leq 1$, and $\bar{F}(\bar{\mathbf{v}})=0$ for $|\bar{\mathbf{v}}|>1$, where $\bar{\mathbf{v}}$ is the normalized particle speed. Due to distribution isotropy only the term $l=0$ needs to be retained in the multipole-expansion boundary conditions. The results of the COGENT simulations for the second Rosenbluth potential [Fig. 2(b)] are compared with the free-space analytical solution to Eqs. (5)-(6), and second-order accuracy of the numerical solution is demonstrated [Fig. 2(c)].

The asymptotic convergence of the multipole-expansion boundary conditions is illustrated in Fig. 3. For this test-case, the normalized distribution function in Fig. 2(a) is shifted in the direction of the normalized parallel velocity by $\bar{v}_0=0.35$ [Fig. 3(a)]. As expected, the numerical solution for the Rosenbluth potentials converges to the correspondingly “shifted” analytical free-space solution provided a sufficient number of multipole terms is retained in the multipole-expansion boundary conditions [Figs. 3(b) and 3(c)].

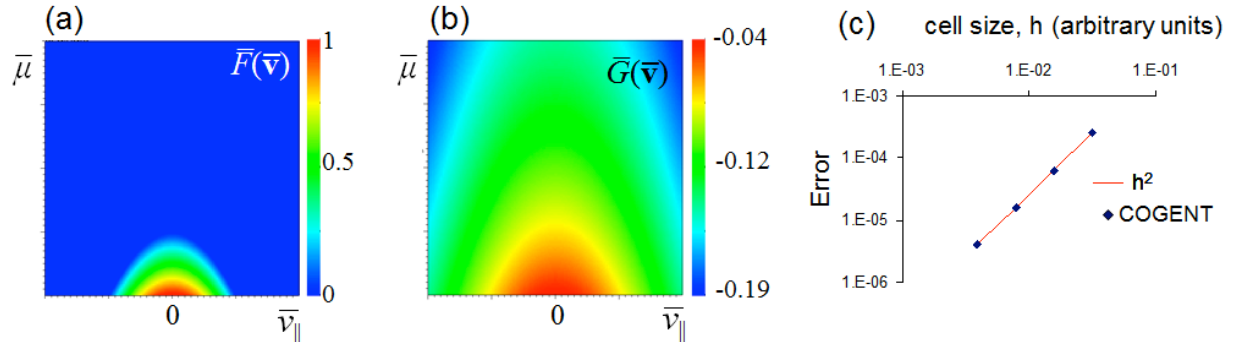


Fig. 2 COGENT evaluation of the Rosenbluth potentials. Shown are (a) the normalized distribution function $\bar{F}(\bar{\mathbf{v}})$; (b) the normalized COGENT solution for the second Rosenbluth potential [Eq. (6)]; and (c) the numerical error (blue dots) defined by the maximal difference between the analytical and COGENT solutions to Eq. (6). The cell size parameter, h , is measured by $1/N^{1/2}$, where N is the total number of velocity grid points to represent the distribution function and the same number of grid points in v_{\parallel} and μ directions is used in the simulations. The simulations are performed for $N^{1/2}=\{32,64,128,256\}$. The red line corresponds to a second-order convergence rate.

After testing the evaluation of the Rosenbluth potentials, we now perform more comprehensive verification studies, in which Maxwellian relaxation of an arbitrary distribution function is investigated [Fig. 4]. For this test, the gyro-kinetic advection operator is turned-off, and the simulation model is given by

$$\partial F / \partial t = C[F], \quad (19)$$

where $C[F]$ is the Fokker-Plank collision operator specified in Sec. 2. The initial distribution function is taken to

be $F(\mathbf{v}) = A \exp(-B|\mathbf{v}|^4)$, where A and B are the normalization constants. Figure 4 shows that the distribution relaxes to a Maxwellian distribution with the same energy and parallel momentum. In addition, second-order accuracy in energy conservation is demonstrated [Fig. 4(c)].

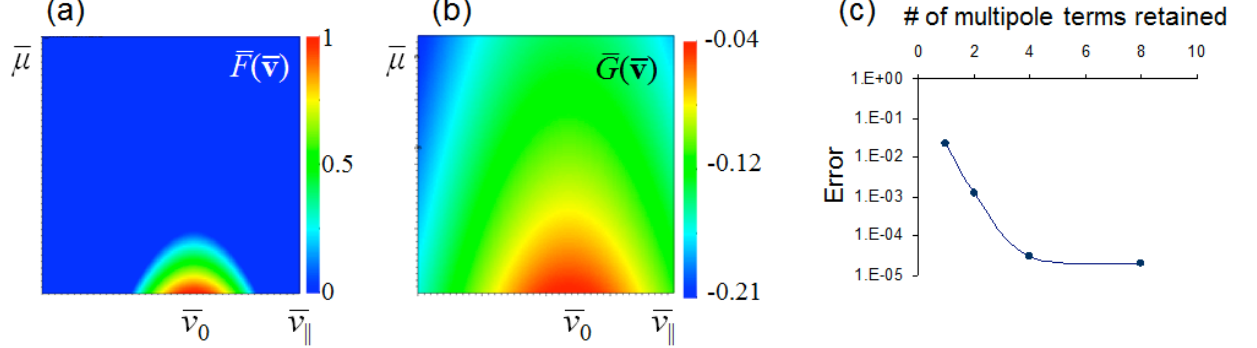


Fig. 3 Convergence of the multipole-expansion boundary conditions. Shows are (a) the normalized distribution function $\bar{F}(\bar{\mathbf{v}})$; (b) the normalized COGENT solution for the second Rosenbluth potential [Eq. (6)]; and (c) the numerical error defined by the maximum difference between the analytical and COGENT solutions to Eq. (6). The simulations are performed for $N^{1/2}=128$ (with the same number of grid points in $v_{||}$ and μ directions), and the error saturation in frame (c) corresponds to the finite (second-order) accuracy of the numerical discretization shown in Fig. 2(c).

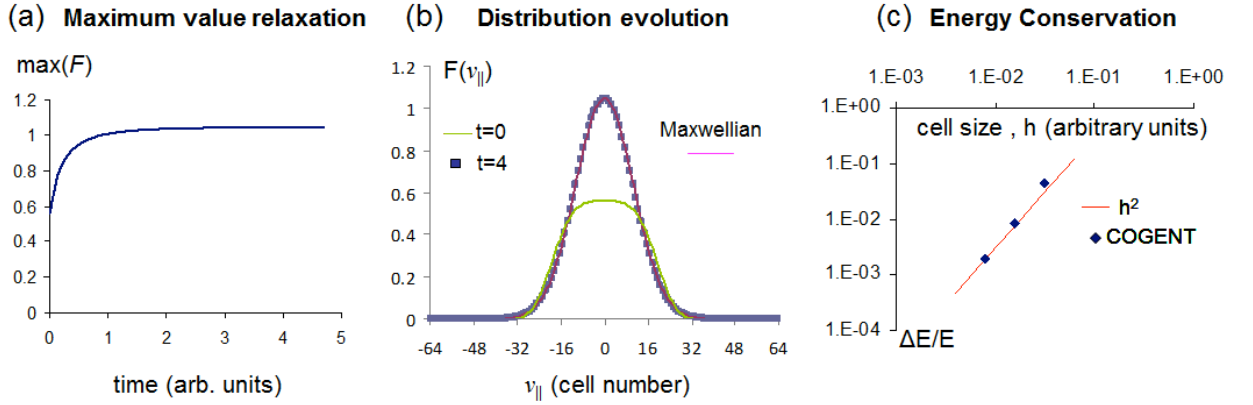


Fig. 4 Verification studies of the Fokker-Plank operator: Maxwellian relaxation. Shown are (a) time-evolution of the maximum value of the distribution function $F(\mathbf{v})$; (b) $v_{||}$ -slice of the distribution function corresponding to the time instances of $t=0$ (green curve) and $t=4$ (blue dots), and a Maxwellian distribution fit (pink line); and (c) normalized energy error (blue diamonds) accumulated over a time period of $t=4$ for the grid resolutions corresponding to $N^{1/2}=32, 64$, and 128 (with the same number of grid points in $v_{||}$ and μ directions). The energy error ΔE is normalized to the corresponding initial value, E . The red line corresponds to a second-order convergence rate. The results in Frames (a) and (b) are obtained using $N^{1/2}=128$.

4 Conclusion

We report on extending the COGENT code capabilities by including the fully nonlinear Fokker-Plank collision model for edge plasma simulations. The presence of velocity-space holes in a tokamak edge plasma distribution may significantly degrade the converging properties of spectral techniques, which are often used for the evaluation of the FP operator in a tokamak core. This issue motivates development of finite-difference schemes that can significantly benefit from the AMR capabilities that are provided by the CHOMBO framework [6] on which COGENT is built. Here, for preliminary studies we develop a finite-difference algorithm for evaluating the Rosenbluth potentials on a uniform ($v_{||}$ - μ) grid. Evaluation of the Rosenbluth potentials requires solving two Poisson equations in the open velocity space, and therefore the appropriate boundary conditions should be computed for a finite-domain simulation. In contrast to the numerical schemes involving spectral decomposition,

finite-difference algorithms lack natural free-space boundary conditions. As a result, the Rosenbluth potentials have to be evaluated at the domain boundaries by making use of the free-space Green's function method. However, direct computation of the corresponding Green's function integral can be computationally more intensive than the iterative solve itself, and thus we develop a multipole-expansion-based approach for evaluating the boundary conditions. The approach is implemented in COGENT and is successfully verified. Potential numerical error introduced by "cut-cells" related to the natural coordinates of the multipole-expansion (i.e., v and $v_{||}/v$) not being conformal to the $(v_{||}, \mu)$ COGENT grid, is pointed out and discussed.

Acknowledgments This work was performed under the auspices of the U.S. Department of Energy at Lawrence Livermore National Laboratory under contract DE-AC52-07NA27344.

References

- [1] M. A. Dorf et al., *Contrib. Plasma Phys.* **52**, 518 (2012).
- [2] M. A. Dorf et al., *Phys. Plasmas* **20**, 012513 (2013).
- [3] M. A. Dorf et al., *Nucl. Fusion* **53**, 063015 (2013).
- [4] M. R. Dorf et al., in: *Proceedings of the SciDAC 2010 Conference*, Tennessee 2010.
- [5] P. Colella et al., *J. Comput. Phys.* **230**, 2952 (2011).
- [6] P. Colella et al., *Chombo Software Package for AMR Applications-Design Document*. <http://seesar.lbl.gov/anag/chombo>.
- [7] E. A. Belli and J. Candy, *Plasma Phys. Control. Fusion* **54**, 015015 (2012).
- [8] M. G. McCoy et al., *Comput. Phys. Commun.* **24**, 37 (1981).
- [9] M. Landreman and D. R. Ernst, *Plasma Phys. Control. Fusion* **54**, 115006 (2012); *J. Comput. Phys.* **243**, 130 (2013).
- [10] A. Pataki and L. Greengard, *J. Comput. Phys.* **230**, 7840 (2011).
- [11] L. Chacon et al., *J. Comput. Phys.* **157**, 618 (2000).
- [12] Y. Saad, *Iterative Methods for Sparse Linear Systems* (PWS, Boston, 1996).
- [13] Hypre library is a software product of LLNL, CA, USA (<http://www.llnl.gov/CASC/hypre/>).
- [14] J. Jackson, *Classical Electrodynamics* (John Wiley & Sons, Inc. 1962).